Intracellular Trafficking and Subcellular Distribution of a Large Array of HPMA Copolymers

ARTICLE *in* BIOMACROMOLECULES · JULY 2009

Impact Factor: 5.75 · DOI: 10.1021/bm801514x · Source: PubMed

3 AUTHORS, INCLUDING:

Jon Callahan
University of Utah
7 PUBLICATIONS **231** CITATIONS

SEE PROFILE

Published in final edited form as:
Biomacromolecules. 2009 July 13; 10(7): 1704–1714. doi:10.1021/bm801514x.

Intracellular Trafficking and Subcellular Distribution of a Large Array of HPMA Copolymers

Jon Callahan[†], **Pavla Kopečková**[‡], and **Jindřich Kopeček**[*,†,‡]
Departments of Bioengineering and Pharmaceutics and Pharmaceutical Chemistry, University of Utah, Salt Lake City, Utah 84112

Abstract

The basic physicochemical properties that determine the distribution and fate of synthetic macromolecules in living cells were characterized using fluorescently labeled HPMA (*N*-(2-hydroxypropyl)methacrylamide) copolymers. Twelve different classes of water-soluble copolymers were created by incorporating eight different functionalized comonomers. These comonomers possessed functional groups with positive or negative charges or contained short hydrophobic peptides. The copolymers were fractionated to create parallel “ladders” consisting of 10 fractions of narrow polydispersity with molecular weights ranging from 10 to 200 kDa. The intracellular distributions were characterized for copolymer solutions microinjected into the cytoplasm of cultured ovarian carcinoma cells. Even the highest molecular weight HPMA copolymers were shown to quickly and evenly diffuse throughout the cytoplasm and remain excluded from membrane-bound organelles, regardless of composition. The exceptions were the strongly cationic copolymers, which demonstrated a pronounced localization to microtubules. For all copolymers, nuclear entry was consistent with passive transport through the nuclear pore complex (NPC). Nuclear uptake was shown to be largely dictated by the molecular weight of the copolymers, however, detailed kinetic analyses showed that nuclear import rates were moderately, but significantly, affected by differences in comonomer composition. HPMA copolymers containing amide-terminated phenylalanine-glycine (FG) sequences, analogous to those found in the NPC channel protein, demonstrated a potential to regulate import to the nuclear compartment. Kinetic analyses showed that 15 kDa copolymers containing GG**FG**, but not those containing GGL**FG**, peptide pendant groups altered the size-exclusion characteristics of NPC-mediated nuclear import.

Introduction

Water-soluble, synthetic polymers have been successfully used in a variety of applications to enhance the delivery and efficacy of therapeutic drugs, nucleic acids, peptides, and proteins. For example, polymeric anticancer drug carriers have been used to greatly enhance the biocompatibility,[1,2] pharmacokinetics,[3,4] nonimmunogenicity,[2,5] and cell targetability[6–10] of chemotherapeutic agents, while reducing their toxicity toward normal tissues.

[*]To whom correspondence should be addressed. Phone: (801) 581-7211. Fax: (801) 581-7848. jindrich.kopecek@utah.edu.
[†]Department of Bioengineering.
[‡]Department of Pharmaceutics and Pharmaceutical Chemistry.

Supporting Information Available. Uptake of copolymers in MDAH2774 cells (Figure S1) and movies S1–S7 depicting the fate of HPMA copolymers after microinjection into the cytoplasm of MDAH2774 cells. This material is available free of charge via the Internet at http://pubs.acs.org.

Typically, cell uptake of synthetic macromolecules occurs via endocytosis, whereby high molecular weight molecules are routed to the lysosomal compartment. Pharmaceutical activity necessitates the subsequent release of the active agent from the endocytotic vesicles. For polymer–low molecular weight drug conjugates, release of the drug from the polymeric carrier can be accomplished by the use of hydrolyzable bonds. The delivery of intact macromolecules directly to the cytosol of target cells has been accomplished by a variety of methods that destabilize lipid membranes.[11]

Once macromolecules are delivered to the cytosol, a number of methods may be employed to traffic them to specific subcellular compartments, such as the nucleus and mitochondria, to enhance their therapeutic efficacy. Nuclear and mitochondrial localization of macromolecules has been mediated by targeting peptides[12–15] or the lipophilic triphenylphosphonium cation.[16–18]

However, macromolecules (without subcellular targeting moieties) are typically excluded from entering membrane-limited organelles, such as mitochondria, lysosomes, the endoplasmic reticulum, in a nonspecific manner. The exception to this is the nucleus whose membrane possesses channels that allow the passive uptake of intermediate-sized macromolecules. The NPC (nuclear pore complex) of the nuclear envelope is composed of about 30 different nucleoporin proteins and is the conduit for both nuclear import and export of macromolecules, such as proteins and nucleic acids. In active transport, cargo as large as 40 nm possessing NLS (nuclear localization sequence) or NES (nuclear export sequence) signaling peptides are guided through the channel after binding to NTR (nuclear transport receptor) proteins.[19] For smaller macromolecules below 10 nm, however, NPCs have been shown to act as nonspecific pores that allow exchange between the nucleus and cytoplasm by diffusion.[20] As a conduit for nonbiological macromolecules, the NPCs have been shown to transmit PEG-coated gold colloid particles 4–7 nm in diameter.[21] In contrast, 27 and 39 nm PEG-gold particles and 25 nm quantum dot particles conjugated with NLS peptide sequences have been shown to require the active nuclear import mechanism for uptake by the nucleus.[19,21,22]

Recent dynamic structural modeling of several of the nucleoporins in the core of the NPC has been used in an attempt to explain the dual size selection of active versus passive nuclear transport selection.[23] The structure of several nucleoporins notably contains natively unfolded domains containing hydrophobic FG (phenylalanylglycine) domains, consisting of FG, GLFG, and FXFG peptide repeats. Several different models are currently under debate to account for the dynamics of NPC transport. Ribbeck et al. have proposed that the FG domains form a polymer brush conformation in the NPC channel that excludes larger solutes by entropic hydrophobic repulsion.[24,25] Frey et al. have suggested that nucleoporins form an unstructured hydrogel mesh in the core of the NPC channel through reversible cross-links of FG peptide repeats that they possess.[26,27] Nuclear import proteins have been shown to possess a number of hydrophobic regions that specifically bind to nucleoporins in their FG repeat regions and have been proposed to disassociate interchain cross-links. The pore proteins, thereby, form a 3-dimensional mesh with a simple molecular weight permeability cutoff when cross-linked. In this model of active transport, NTRs are able to open the nucleoporin mesh by “melting” the hydrogel structure and guide large macromolecules in or out of the nuclear compartment.[28] Alternately, Melčák et al. have proposed that the interface between the α-helical regions of nucleoporins selectively slide circumferentially to dilate the NPC pore opening after NTR binding.[29]

Nonetheless, relatively little is known about the chemical and physical forces that direct localization of macromolecules once in the cytosol. To help ascertain this basic understanding, we took advantage of a well-characterized and synthetically flexible polymer

system to create an array of macromolecules with widely divergent chemical characteristics. Fluorescently labeled *N*-(2-hydroxypropyl)methacrylamide (HPMA) copolymers with a reproducible range of well-defined molecular weights were made using comonomers with a variety of charges and hydrophilicities in an attempt to reveal the physicochemical properties that guide the intracellular transport and distribution of synthetic macromolecules. The copolymers were fractionated into a series of polymers of narrow polydispersity and microinjected into the cytosol of cultured human ovarian carcinoma cells. Their fate was observed using fluorescence microscopy and other imaging methods. A variety of subcellular markers were simultaneously used to identify subcellular compartments within the cells to determine colocalization. Specific issues investigated included: diffusion in the cytoplasm, relative rates of nuclear entry, binding to intracellular membranes and other structures, and sequestration by subcellular compartments.

Finally, HPMA copolymers containing FG (Phe-Gly) motifs were generated in an attempt to modulate the kinetics of nuclear uptake of macromolecules. Their structure was based on recent theories describing the function of proteins of the NPC (nuclear pore complex) in the nuclear membrane that have been shown to regulate nuclear import and export of macromolecules.

Experimental Section

Monomers

All chemicals and solvents used were of reagent grade or better unless otherwise stated. MAA (methacrylic acid), DEMA (2-(*N*,*N*-dimethylamino)ethyl methacrylate), and SEMA (2-sulfoethyl methacrylate) were purchased from PolySciences, Inc. HPMA (*N*-(2-hydroxypropyl)methacrylamide)[30] and MA-FITC (*N*-methacrylolyaminopropyl fluorescein thiourea)[31] were prepared as previously described. MATC (*N*-methacryloyloxyethyl trimethylammonium chloride) was prepared as described before by quaternization of DEMA with gaseous methylchloride in acetone.[32] The peptide monomers *N*-methacryloylglycylglycine (MA-GG), *N*-methacryloylglycylphenylalanine (MA-GF), and *N*-methacryloylglycylphenylalanylleucylglycine (MA-GFLG) were prepared as described previously.[33]

The amide-terminated monomers MA-GGFG-NH_2 (*N*-methacryloylglycylglycylphenylalanylglycine amide) and MA-GGLFG-NH_2 (*N*-methacryloylglycylglycylleucylphenylalanylglycine amide) were synthesized using standard Fmoc solid-phase peptide chemistry. On Rink Amide MBHA resin (Novabiochem), glycine and phenylalanine or glycine, phenylalanine, and leucine were sequentially attached. While still conjugated to the resin, the peptides were coupled to *N*-methacryloylglycylglycine peptide (MA-GG). The completed monomers were then released using a TFA solution and precipitated in diethyl ether. The dried monomers were purified using RP-HPLC, and their mass verified using MALDI-TOF MS. The molecular masses for the two main ion peaks measured for MA-GGFG-NH_2 were 404.2 and 426.2, corresponding to calculated values 404.4 ($M{\cdot}H^+$) and 426.4 ($M{\cdot}Na^+$). The molecular mass of the main ion peak measured for MA-GGLFG-NH_2 was 539.3 versus a calculated value of 539.5 ($M{\cdot}Na^+$).

Polymer Chemistry

All copolymers used in this study were generated by radical chain polymerization using 0.60 wt % AIBN as the initiator. The feed mole ratios of all 12 copolymerizations and copolymer compositions are shown in Tables 1 and 2. The structure of monomers and copolymers is depicted in Scheme 1. (For the sake of clarity, all polymers were named based on the concentration of feed comonomer rather then final content in the copolymers.) Methanol was used as the bulk solvent for all reactants of the polymerization in a total reaction volume

of 5 mL. To slightly lower the average molecular weight of each of the resulting copolymers, 0.078 wt % mercaptopropionic acid was added as a chain transfer agent. Before mixing with the other components of the polymerization reaction, some of the monomers were first dissolved in other solvents to ensure complete dissolution. The liquid monomer SEMA was diluted 1:10 with water to ensure miscibility with methanol during the polymerization reaction. The peptide monomers MA-GFLG, MA-GF, MA-GGFG-NH_2, and MA-GGLFG-NH_2 were dissolved in a minimum volume of DMSO (~2 μL/mg) before addition to the reaction solution. The alkaline monomers DEMA and MATC were dissolved in 0.05 N HCl_{aq} to a monomer concentration of 250 mg/mL to acidify the final reaction solution.

After mixing, the polymerization solutions were bubbled with argon, sealed in a glass ampule, and then heated to 50 °C for 24 h. When complete, the reactions were dried under vacuum and then redissolved in a minimum volume of methanol. The polymers were then separated from the unreacted monomers on an LH-20 column with methanol as the mobile phase. The eluted fractions containing the FITC-labeled product were then dried under vacuum, redissolved in a minimum amount of distilled water, and then freeze-dried to isolate the finished solid product. The final yields of all copolymers were between 75–85%.

Texas Red-Labeled HPMA Copolymer

HPMA copolymer labeled with Texas Red (Table 2) were synthesized in a two-step process, as previously described.[34] First, a copolymer of HPMA with *N*-(3-aminopropyl)methacrylamide (molar ratio 98:2) was synthesized by radical copolymerization. The copolymer contained 1.9 mol % of amine side chains; M_w = 80000. In the second step, Texas Red was attached by the reaction of Texas Red succinimidyl ester (Molecular Probes) with amine groups of the copolymer. The purified product contained 1.6 mol % Texas Red containing side chains as determined spectro-photometrically (η = 86000 M^{-1} cm^{-1}, 593 nm, PBS).

Copolymer Characterization

For all FITC-labeled copolymers, the content of MA-FITC monomer was determined by spectrometry using the absorbance at 495 nm ($\eta_{495\ nm}$ = 80000 M^{-1} cm^{-1}) in 0.1 M borate buffer (pH 9). The content of peptide monomer in the six peptide-containing copolymers was determined by HPLC amino acid analysis (AAA) using phenylalanine as a reference. For this, 2–3 mg of peptide-containing copolymer was hydrolyzed in 0.2 mL of 6 N HCl in a sealed glass ampule at 115 °C for 16 h. The hydrolyzate was dried over NaOH pellets in vacuo and then dissolved in 0.5 mL of distilled H_2O. Before separation on a reverse phase Microsorb MV C18 column, the amino acids in the sample were derivatized with *o*-phthaldialdehyde (OPA). HPLC used a 10–90% gradient elution where solvent A was 0.05 M sodium acetate in 0.25% acetonitrile pH 6.0 and solvent B was 0.05 M sodium acetate in 70% acetonitrile. The HPLC fluorescence detector used the excitation at 229 nm and emission at 450 nm. The content of charged MAA, SEMA, and DEMA comonomers was determined using an automated TIM854 pH titration workstation (Titralab, Radiometer Analytical, Lyon, France) with a combined minitype electrode and either 0.05 N NaOH or 0.05 N HCl as a titration standard solution. Content of MATC was determined by potentiometric titration of chloride ions using a combined silver type electrode and 0.05 M $AgNO_3$ titration standard solution. The comonomer content and characterization of the copolymers are summarized in Tables 1 and 2.

Size-exclusion chromatography (SEC) was used to determine the molecular weight distribution of the polymers. All samples were run on an FPLC system (GE Healthcare) equipped with UV and differential refractive index detectors using a Superose 6 HR10/30

analytical column in PBS (pH 7.3) calibrated with polyHPMA standards of a narrow polydispersity ($M_w/M_n < 1.2$). To ensure accurate molecular weight calculations, polymer size was also calculated using dynamic light scattering in tandem with SEC. For this, d*n*/d*c* measurements were determined for each polymer with a DSP interferometric refractometer (OPTILAB, Wyatt Technology, Santa Barbara, CA) using standard polymer/PBS solutions. Molecular weight determinations were made using laser light scattering data (MINIDAWN, Wyatt Technology) and calculated using chromatographic software (ASTRA, Wyatt Technology).

Copolymer Fractionation

All 12 copolymers were further fractionated into a standard molecular weight "ladder" series using a preparative Superose 6 HR16/60 FPLC column. For each separation, 50 mg of polymer was loaded on to the column using PBS as the eluent and a flow rate of 1 mL/min. Fractions were collected using the same schedule for all copolymers, whereby 10 fractions of 5 mL each were taken during the 50 min window of polymer elution from the column. At least two 50 mg fractionations were performed for each copolymer. The corresponding fractions for each separation (labeled F1–F10 for fractions 1–10) were pooled, dialyzed extensively against water, and freeze-dried. The molecular weight distributions of the resulting polymer fractions were then characterized using a Superose 6 analytical SEC column. A summary of the molecular weight analyses for the fractions used in subsequent experiments are shown in Tables 1 and 2. Analyses of the content of comonomer for several randomly selected copolymer fractions were analyzed using pH titrations, AAA and AgCl titration to ensure that the mole fractions of the fractionated polymers were similar to that of the starting unfractionated polymers.

Cell Culture

MDAH2774 ovarian carcinoma cells (ATCC) were cultured in Lebowitz's L-15 media supplemented with 10% fetal bovine serum (HyClone Laboratories, Logan, UT) and 10 μg/mL insulin (HyClone) and 12.5 mM HEPES buffer (pH 7.4) under a humidified atmosphere at 37 °C. One day prior to each study, 50000–100000 cells were seeded on coverslip microwell dishes. For static imaging studies, cells were seeded in No. 1.5 glass-bottom 14 mm microwell dishes (MatTek Corp., Ashland, MA). For time-lapse experiments, cells were seeded on 0.17 mm Delta T temperature-controlled microwell dishes (Bioptechs, Inc., Butler, PA).

In colocalization studies, fluorescent subcellular markers were used. For these, media containing the markers was added approximately 1 h before initial imaging, and fresh media was added to the microwell dishes immediately before imaging. To identify mitochondria, 100 mM MitoTracker Orange CM-H_2TMRos (Molecular Probes) was added. To identify lysosomes, 50 mM LysoTracker Red (Molecular Probes) was used.

Live Cell Imaging

Live cell polymer uptake studies were conducted using scanning laser confocal fluorescence microscopy (Olympus Flowview with krypton/argon excitation lasers). For static microscopy, images were collected by combining dual-channel fluorescent and transmitted light using z-series slices in 0.2 μm steps. Image data was processed using ImageJ software.

Incubation of MDAH Cells with Copolymers Dissolved in Media

As a control to determine the baseline mode of polymer internalization, MDAH ovarian carcinoma cells (ATCC) were incubated with each of the polymers in their incubation media. A single molecular weight fraction (fraction 9, all ranging in average molecular

weights between 12–17 kDa) of each polymer type was used in a systematic study of uptake. Plated cells were incubated for 24 h in growth media containing 0.5 mg/mL polymer. Before imaging the media was replaced with fresh media. The cells were then imaged using confocal laser scanning microscopy (see Figure S1).

Microinjection

Fluorescently labeled 1.0 mg/mL polymer/PBS solutions were directly injected into the cytosol of plated MDAH2774 cells using 0.5 μm glass needles equipped on an Eppendorf Transjector 5346 pressure injector and fixed to an Eppendorf 5171 micromanipulator arm. Pressures used varied from 80 to 120 hPa and care was taken to inject solutions as far from the cell nuclei as possible to avoid traumatizing the cells.

Intracellular Distribution of Copolymer Fractions

Following microinjection, MDAH2774 cells were observed periodically (every 10 or 15 min) for up to 48 h using laser scanning fluorescence confocal microscopy. For detailed comparisons of the effect of molecular weight, every fraction from polymers 5% MAA-P, 5% GFLG-P, and 20% DEMA-P was used.

The distribution of all types of polymers that were completely excluded from nuclei was characterized by injecting MDAH2774 cells with every F4 polymer, which all possessed molecular weights greater than 75 kDa. Cells were microinjected and then incubated at 37 °C for 24 h. At 1 h before imaging, either LysoTracker Red or MitoTracker Orange (Molecular Probes) was added to the media. Immediately before imaging, the media was replaced with fresh media.

Rates of Nuclear Entry/Time Lapse Imaging

F7 (fraction 7) polymers of a uniform molecular weight (M_w = 36 ± 6 kDa) of 5% comonomer polymers were selected. To quantify the rate of nuclear entry, time-lapse imaging was performed on MDAH2774 cells after microinjection. Each movie was started 10–15 min after polymer microinjection. Each frame of the movies represents 15 min (or 10 min in the case of polymers MAA-P, MATC-P, and GFLG-P) and they were collected until there was an apparent equilibrium between the nuclear vs cytosolic concentrations. Laser power was set low (2–5%) to minimize bleaching during imaging. The image series used for measurement was of one confocal plane taken approximately midway through the nuclei or 2–4 μm above the coverslip surface. For quantification analysis, the image series was coded and the fluorescent image intensity data were collected by a blinded second party. Cells in the image series were numbered and tracked separately during the movie to account for cell migration and changes in cell shape. For each polymer, 5–9 cells in the series in the imaging frame were used in the analysis. Polymer concentrations in the nuclei and cytosol were measured by the image intensity of 2 μm radii circular regions in the nuclei and the perinuclear cytosol of each cell. The regions used for measurement were manually moved during the series to account for cell movement. Nuclear entry time courses of each cell measured for each polymer were averaged and then curve-fitted by regression analysis using SigmaPlot software to a three-parameter rising exponential function of the form:

$$R_{n/c}=R_0+R_{eq}\times(1-e^{-kt}),$$

$R_{n/c}$ is the ratio of the nuclear versus cytosol polymer concentration, R_0 is the fitted initial N/C ratio (to account for background fluorescence in measured values), R_{eq} is the equilibrium concentration of polymer in the nucleus versus cytosol, and k (min^{-1}) is the rate constant of nuclear uptake. To evaluate statistically significant differences, the nuclear entry rate

constants for all test polymers were compared to the rate constant calculated from control polyHPMA-FITC using the two-tailed Student's *t* test. Differences in mean values were considered significant for P-values less than 0.05.

Fluorescence Recovery After Photobleaching (FRAP)

FRAP was performed on MDAH2774 cells after cytosolic microinjection of copolymers. In each study, polymer was injected 1–2 h before the bleaching experiment. Imaging was performed on a FV1000 Olympus confocal microscope with an independent light path and galvo SIM scanner (simultaneous image microscopy) image scanning system. An ~2 μm diameter spot was bleached for each microinjected cell using a 405 nm diode laser as the light source. Images before, during, and after bleaching were taken every ~0.6 s for several min. In some series, the bleaching laser was turned on continuously to determine whether any copolymer was retained by components of the cell (i.e., FLIP, fluorescence loss in photobleaching).

Coinjection of FG Peptide Copolymers and Nuclear Exclusion Markers

The FG containing polymers were generated to determine whether the peptide pendant groups affected the kinetics of nuclear entry via the NPC. For this, the FITC-labeled, fractionated copolymers were coinjected into MDAH2774 cells with fractionated Texas Red-labeled polyHPMA (TR-P) as a marker for nuclear exclusion and uptake. For each coinjection, PBS solutions of 1 mg/mL FITC test polymer and 1 mg/mL TR-P marker polymer were injected into a field of cells. In separate regions of the same coverslip, the cells were injected with 1 mg/mL solutions of either test polymer (green) or TR-P marker polymer (red) alone, to act as controls. Time-lapse confocal z-series imaging of the injected live cells was immediately initiated after injection. Images were collected using 488 and 543 nm lasers in sequence using the same settings for all three regions of injected cells.

Results and Discussion

Design and Characterization of an HPMA Copolymer Array

A large array of HPMA copolymers was synthesized by radical polymerization (Tables 1 and 2). Eight different methacryloyl-functionalized comonomers were employed to confer different pendant functional groups to the resulting linear polymers (Scheme 1). For each copolymer, 1 mol % of MA-FITC (*N*-methacrylolyaminopropyl fluorescein thiourea) was incorporated for convenient visualization. Monomers with four different types of charged groups were used: MAA (methacrylic acid), a weak acid; SEMA (2-sulfoethyl methacrylate), a strong acid; DEMA (*N*,*N*-dimethylaminoethyl methacrylate), a weak base; and MATC (*N*-methacryloyloxyethyl trimethylammonium chloride), a strong base. Four peptide-containing monomers were used to create relatively hydrophobic copolymers: *N*-methacryloylglycylphenylalanine (MA-GF), *N*-methacryloylglycylphenylalanylleucylglycine (MA-GFLG), *N*-methacryloylglycylglycylphenylalanylglycineamide (MA-GGFG-NH_2), and *N*-methacryloylglycylglycylleucylphenylalanylglycineamide (MA-GGLFG-NH_2). Fractionation using SEC provided 10 molecular weight fractions (F1–F10) each with a narrow polydispersity. The content of the comonomers in the resulting copolymers was typically 75–85% of the mol % of the feed concentration; however, for the sake of clarity, the feed comonomer concentrations were used for the nomenclature of the copolymers. For example, "5% GFLG-P" refers to the peptide copolymer resulting from the copolymerization of 5 mol % MA-GFLG, 94% HPMA, and 1% MA-FITC. SEC-fractionated copolymers were further designated by fractionation order and decreasing molecular weight. For example, the suffix in "5% GFLG-P-F7" refers to the seventh SEC fraction of copolymer 5% GFLG-P (Tables 1 and 2).

The molecular weight profiles of the array copolymers from high (F4), midrange (F7), and low (F9) molecular weight fractions from the array copolymers used in later experiments were characterized by SEC. The middle range of fractions from F5 to F9 formed a molecular weight “ladder” of standard copolymer hydrodynamic sizes, as the differences in average molecular weight for fractions 5–9 from all of the polymers had standard deviations less than ±6%. To illustrate, the SEC profiles for the fractions collected from copolymer 5% MATC-P and its structure are shown in Figure 1.

In summary, a two-dimensional array of HPMA copolymers was generated with 12 distinct chemical characteristics in one dimension, and a discrete sequence of five parallel molecular weights (10–80 kDa) in the other dimension.

Uptake and Trafficking of Polymers From Media

As expected, all copolymers when incubated with MDAH2774 ovarian carcinoma cells were internalized by endocytosis (Figure S1). Punctate staining of all cells after incubation with all of the polymers was consistent with lysosomal compartmentalization. The relative amount of polymer uptaken was also consistent with adsorptive endocytosis with the cationic copolymers showing the greatest amount of uptake and anionic copolymers displaying the least. In no case was there evidence of any endosomal/lysosomal escape of polymer after 24 h.

Cytosolic Microinjection

The subcellular distribution of HPMA copolymers was characterized by pressure microinjecting copolymer solutions directly into the cytosol of cultured cells. For all species of copolymers, diffusion occurred rapidly throughout the cytosol after microinjection and had reached equilibrium within a few minutes required to collect images. The copolymers appeared to be excluded from all membrane-limited subcellular compartments, even after 24 h. The only notable shifts in intracellular distribution were observable in rates of nuclear entry. Here, differences were largely, but not entirely, a function of molecular weight rather than the identity or initial concentration of comonomer. The lowest molecular weight polymers injected (i.e., the “F9” and “F10” fractions), with masses less than 25 kDa, immediately diffused throughout the nucleus after cytosolic injection (Figure 2a). In contrast, the highest molecular weight polymers (>60–80 kDa; up to fraction “F5”) remained completely excluded from the nuclei, even after 24 h (Figure 2b). Polymer fractions in the intermediate molecular weights between 25–50 kDa entered the nuclear compartment in time frames that ranged from 15 min to 12 h. Subsequent experiments were designed to explore in detail the differences between polymers with respect to initial subcellular distribution and fate.

Short-Term Intracellular Distribution

To evaluate polymer diffusion through the cytoplasm, FRAP (fluorescence recovery after photobleaching) experiments were performed on selected polymer samples using high-speed time-lapse imaging. When 2 μm regions of cytoplasm were bleached using a short burst from the laser, the diffusion of the surrounding polymer into the bleached area was very rapid and equilibrium was reestablished in less than 3 s for all polymers types (Figure 3). Subsequent FLIP (fluorescence loss in photobleaching) experiments where laser bleaching was used for several minutes showed that all of the polymers in the cell freely diffused to the bleached region within a few minutes (movie S1). The only exception to this trend was observed when using copolymers possessing intermediate molecular weights (25–50 kDa) able to enter the nucleus but slowly over a period of hours. In these microinjected cells, the polymers disappeared from the cytoplasm within 2–3 min, but the copolymer in the nuclei was retained and remained visible. Continued bleaching produced a very gradual decrease of

polymer in the nuclei as the polymer slowly diffused out of the nuclear compartment and into the cytosol where it could quickly diffuse through the bleached region (movie S2). The rapid and homogeneous diffusion of HPMA copolymers as large as 100 kDa throughout the cytoplasm is in good agreement with previous studies of the diffusion of biological macromolecules such as dextran and Ficoll.[35–37] On the contrary, theories on the hydrogel nature of the cytoplasm seem not to hold.[38]

The FLIP experiments using intermediate molecular weight (25–50 kDa) copolymers also confirmed that the only barriers to the free diffusion of most of the polymers were subcellular membrane structures. Furthermore, all of the results with respect to nuclear uptake and export were consistent with simple size-limited unassisted diffusion through the nuclear pore complex.[39,40] Transport in and out of the nuclear compartment was thus symmetrical and consistent with the known properties of passive NPC transport, as opposed to active import or the result of disruption of the nuclear envelope.

Long-Term Intracellular Distribution

The systematic analysis of the long-term fate of the copolymers used fractions with molecular weight averages greater than 80 kDa to avoid potential toxicity. This issue was illustrated in a time-lapse imaging of cells injected with the strongly cationic copolymer 20% MATC–P-F7 (movie S3), which showed the cells collapse and die immediately after the copolymer began to enter the nucleus of each cell, 1–3 h after microinjection.

Use of the organelle markers for mitochondria and lysosomes showed no colocalization using polymers of any of the 10 types studied here, even 24 h after microinjection (data not shown). Further, the only cells that showed significant distributional nonhomogeneity in the cytoplasm were the highly cationic types, particularly 20% MATC-P. As shown in Figure 4, this polymer clearly localized to microtubules, as confirmed by colocalization with antitubulin antibodies. Much weaker microtubule localization was also noted for polymers 5% MATC-P and 20% DEMA-P. In each of these experiments, fluorescent staining of microtubules was a slow process and required several hours of to become observable. Microtubule binding is consistent with the known cation-binding properties of tubulin proteins.[41,42]

Nuclear entry of copolymers was largely dictated by molecular weight rather than chemical composition. Copolymers with intermediate molecular weights between 25–50 kDa entered the nuclei, but slowly, over the course of 15 min to 24 h. The hydrodynamic diameters of charged HPMA copolymers in this mass range have been shown to be between 2–4 nm in free aqueous solution,[43] a range consistent with passive diffusion through the NPC. Systematic time-lapse imaging was then performed on each type of copolymer using size fractions near the cutoff for entry. By using polymers near the nuclear uptake size limit, differences in the rate of nuclear uptake due to *chemical composition* might be characterized.

Kinetics of Nuclear Entry of Copolymers

The use of well-characterized synthetic macromolecules with well-controlled molecular size permitted to better characterize the passive transport characteristics of the NPC. Macromolecular size and shape of HPMA copolymers could be held constant while the chemical functional groups were altered. Because all of the copolymers were charged and relatively hydrophilic, they were all assumed to possess a similar extended, random coil structure in solution, given the presence of counterions. Small changes in import kinetics could be detected and attributed to surface chemical interactions apart from the dimensions of the macromolecules. To this end, time-lapse imaging of MDAH2774 cells after cytosolic

injection was performed using all of the intermediate-sized F7 fractions of the 5% copolymers (M_w = 36 ± 6 kDa) in the polymer array. This copolymer size range has been shown in preliminary studies to enter the nucleus in a time range of 1–6 h, a window convenient for reproducible image analyses. Samples from the time-lapse imaging are shown in Figure 5 for copolymer 5% GFLG-P-F7.

For comparison, fractionated polyHPMA was used as a control (movie S4). Imaging of the cells injected with control (neutral) homopolymers was taken rapidly (3 min/frame) to create a baseline with a minimized experimental error. Cells microinjected with HPMA copolymers were imaged using longer time intervals (10 or 15 min/frame). The time-lapse movies of the cells after microinjection of each of the six types of polymer revealed a large amount of both qualitative and quantitative data, and examples of the resulting time-lapse imaging sequences can be found in movies S5 and S6.

In all cases, copolymer entry into the nucleus was consistent with first-order kinetics and the data was fit to rising exponential functions (Figure 6). *P* values for calculated equilibrium N/C (nuclear/cytoplasmic) ratios (R_{eq}) and import rate constants (k) were typically 0.001 or less. For all polymer types the final equilibrium ratios of nuclear versus cytoplasmic concentrations were less than unity, and ranged between 0.4 and 0.9. Since the polymers possessed some polydispersity and the average M_w varied between polymer types, one possibility was that these differences in equilibrium concentration reflected a fixed molecular cutoff for polymer entry, however, there was no statistical correlation between polymer molecular weight distribution (SEC) and the equilibrium nuclear to cytosol concentration ratio (data not shown).

Overall, the calculated nuclear import rate constants and equilibrium nuclear concentration ratios were significantly different between copolymer types. The calculated import rate constant (k) for the control polyHPMA polymer was 0.0454 min^{-1}, corresponding to a relatively rapid time (1–2 h) for uptake. The only two copolymers with statistically equivalent import rates were the two weakly charged copolymers 5% MAA-P and 5% DEMA-P, with similar rate constants. Forming another distinct group, the two strongly ionic copolymers and the hydrophobic 5% GF-P copolymer had import times which were significantly longer than the control polyHPMA, between 2–3 h. Interestingly, the hydrophobic 5% GFLG-P peptide copolymer had the longest import requiring 4–5 h to reach equilibrium. In general, the kinetics of uptake of the different copolymers were found to be moderately, but significantly affected by their respective chemical characteristics. The weakly charged hydrophilic copolymers were found to possess uptake kinetics little different than the polyHPMA control.

It can be concluded that the kinetics of nuclear entry of copolymers with different chemical compositions became distinguishable as the molecular weight of the polymers approached the size limit for passive diffusion through the NPC. It is possible that the hydration layer effects of the proteins and copolymers may have played a general role in transport rates. The “uncharged” polyHPMA control polymer and weakly ionic copolymers had the fastest transport rates, and decreased charge in the hydrophobic environment of the pore may account for more free movement. The two strongly ionic copolymers had permanent charges, and repulsion from these charges may have created a barrier to transport by reducing partition into the hydrophobic NPC pore environment. It is also possible that the different copolymers may preferentially associate with proteins or other biological agents in the cell that may have greatly changed their hydrodynamic size or their relative affinity for the nucleoporins (Nups), the proteins that compose the internal structure of the NPC channel. Alternately, the slower transport rates for the peptide copolymers may reflect a higher interaction between the polymers and Nups, where the higher hydrophobicity of the

peptide copolymers produced a higher partition ratio into the nuclear channel, but a slower release rate from the interior side of the pore. The low release equilibrium into the nucleoplasm may have presented the rate-limiting step for nuclear entry of the peptide copolymers. Overall, nuclear import may have been optimized for the copolymers with minimal capacity for interaction with biological macromolecules.

The results of nuclear import kinetics using copolymers with GF and GFLG peptides, GF-P and GFLG-P, was of particular interest to recent work in modeling the dynamics of the structure of Nups to explain the dual size selection of active versus passive nuclear transport selection by the NPC. The structure of Nups is most notable due to the role natively unfolded domains play in controlling NPC transport kinetics.[24–29,44,45] These unfolded domains are referred to as FG-regions due to their characteristic hydrophobic repeat peptide sequences containing FG, frequently including GLFG, and FXFG. It was by happenstance that two of the HPMA copolymers used in the initial cohort of samples in this study possessed similar (though inverted) peptide sequences, GF and GFLG. Furthermore, the average half-life of nuclear entry of the peptide copolymers (but not the molecular weight cutoff) was significantly higher, particularly for the GFLG copolymer. The overall pattern of the rate of nuclear entry was possibly merely a function of the relative hydrophobicity of these polymers. However, the slower import kinetics of the GFLG tetrapeptide copolymer were also suggestive that this polymer may have the ability to interact with proteins in the NPC channel in a specific manner that may resemble Nups or the activity of the Nups-binding proteins responsible for active transport through the NPC (karyopherins). Subsequent experiments with an array of peptide-containing copolymers were designed to explore this possibility further.

Nuclear Transport Modulation with FG-Peptide Copolymers

The 5% GGLFG-P and 5% GGFG-P (Table 2) were selected to evaluate the potential of HPMA copolymers with FG motifs to modulate the kinetics of nuclear uptake. In these copolymers the FG sequence matched the correct sequence directionality of Nups and a spacer between the FG motif and the polymer backbone increased the accessibility for protein binding. Moreover, the peptide side chains were terminated with amides to remove the negative charge that would be directly adjacent to the putative binding sites.

In Figure 7a,b, the calculated nuclear uptake half-lives and equilibrium nuclear/cytosol ratios, respectively, are shown for “F7” fractions of both copolymers after microinjection into the cytosol of MDAH2774 cells. The kinetic results showed that both copolymers displayed extended uptake half-lives similar to those measured for the 5% GFLG-P-F7 copolymer. In contrast, only the 5% GGFG-P-F7 copolymer yielded an equilibrium nuclear concentration significantly higher than that derived for control polyHPMA. These results suggested that the rate of polymer transport through the NPC was affected by the overall hydrophobicity/hydrophilicity of the copolymers rather than by specific peptide interactions with nucleoporin proteins. The higher equilibrium nuclear concentration of the 5% GGFG-P-F7 copolymer, however, raised the possibility that this copolymer affected an increase in the molecular weight cutoff for diffusion through the NPC.

Polymer Coinjections

Because the peptide copolymers are presumed to interact directly with the nucleoporin cross-linking domains, general effects on NPC transport were evaluated using fractionated polyHPMA labeled with Texas Red (TR-P) as nuclear exclusion marker (Table 2).

For time-lapse imaging, FITC-labeled peptide copolymers were injected simultaneously into MDAH2774 cells with TR-P. As controls, separate regions of cells were injected with either

the test or marker copolymers alone. When this approach was used, small changes in the kinetics of transport through the NPC affected by the peptide copolymers could be measured separately from the uptake kinetics of the peptide polymer itself. This precision in the experimental design and use of several types of controls were included to overcome several potential sources of experimental error. Pressure microinjection of high concentrations of the HPMA copolymers introduces a number of factors that may have interfered with the quantization of intracellular polymer concentrations over time. The injected cell's responses to the physical trauma of injection and the dispersal of copolymers may include direct damage to the nuclear membrane, mitosis in the cell, or other stresses that induce apoptosis or necrotic death. All of these can affect the structure of the nuclear envelope and obscure measurements of NPC-mediated nuclear uptake. For these reasons, data was collected from many separate cells and was used only from cells that remained morphologically stable and intact (alive) for the duration of time-lapse imaging. Cells that had very high initial concentrations or sudden increases in nuclear copolymer concentrations were excluded from data analysis.

Assuming that the FG peptide copolymers affect Nup cross-links and that this interaction had a measurable effect on NPC transport, these changes were hypothesized to have several possible manifestations. One was that the copolymers might form their own cross-links with the Nups. If stably cross-linked, the polymers may have had the effect of blocking the NPC pore or tightening a putative hydrogel mesh structure. This may express itself as slowing the rate of pore transport or lowering the molecular weight cutoff of the channel. Alternately, the copolymers may have disrupted the Nup FG-domain cross-links or alter the dynamics of cross-linking. Given the hydrogel model of Nup structure,[24,26,27] a phase transition in the pore structure may be affected similar to the hypothesized mechanisms of active nuclear uptake by importin proteins. These changes may be expressed by increased uptake kinetics or a large increase in the size of macromolecules able to transit the NPC. Because it is known that the larger copolymers contained an increasing number of FG-peptides per polymer chain, different sizes of copolymer were anticipated to have different effects on transport, depending on the model of Nup structure.

Coinjections with the TR-P-F6 (M_w = 45 kDa) marker polymer were performed to better evaluate whether the test copolymers increased the molecular weight cutoff of NPC transport. Because of its molecular weight distribution, TR-P-F6 was largely excluded from passive nuclear uptake for up to 12 h. Preliminary coinjections determined that noticeable increases in nuclear uptake only occurred when the lowest molecular weight fractions (F9) from each peptide copolymer were used. In addition, differences in marker polymer uptake only occurred when the peptide copolymer concentration was higher than a particular threshold. For microinjections using 5% GGFG-P-F9 and 5% GGLFG-P-F9, it was found that polymer concentrations greater than 1 mg/mL were required given microinjection volumes less than 5–10% of the total cell volume, or an intracellular copolymer concentration greater than 50–100 μg/mL. In the final series of coinjection experiments, 5% GGFG–P-F9 (M_w = 15 kDa) and 5% GGLFG-P-F9 (M_w = 14 kDa) were each coinjected with TR-P-F6 marker polymer into MDAH 2774 cells and then imaged for 8–12 h. Differences in the rate of nuclear uptake of the marker polymer were directly derived from a comparison of the coinjected cells and cells injected with the TR-P marker polymer alone. As shown in Figure 8, coinjection with 5% GGFG-P-F9 (but not 5% GGLFG-P) significantly increased the import rate constant and total equilibrium nuclear concentration of TR-P-F6 marker poly-HPMA compared to marker polymer alone. An example of a time-lapse imaging of the coinjected cells is shown in movie S7 that demonstrates this shift. These results showed that the incorporation of FG peptide motif onto HPMA copolymers had a small but measurable effect on the molecular size of solutes able to diffuse into the nuclei of nondividing cells. Although time to reach equilibrium was not increased

significantly, the initial rate of uptake increased more than 3-fold, and the apparent molecular weight cutoff of the NPC channel was effectively increased by 20–30%.

The subtle variations in the kinetics of the different chemical types of copolymers near the molecular weight cutoff of passive nuclear uptake correlate well with the expected differences in binding to the hydrophobic domains of Nups. This observation is consistent with the repulsive exclusion models of NPC gating and passive transport.[46,47] It is also consistent with models of partitioning into the hydrophobic interior of the pore.[48] However, more consensus between all of the competing models of NPC transport is required to fully interpret the meaning of these differences in transport.[49–51] None of the FG-peptide copolymers dramatically increased the rate or the molecular weight limit of nuclear import in a manner that would suggest a complete phase transition of a putative reversible Nup hydrogel. The importance of this is difficult to evaluate since the copolymers did not possess Nup binding sites analogous to those found on karyopherin proteins. Without a direct determination of the binding affinity between the copolymers and the Nups, it is difficult to evaluate the implications of unaltered uptake dynamics. The most striking result, however, was the shift in the molecular weight cutoff of nuclear uptake affected by low molecular copolymers containing GGFG peptides. This shift in NPC dynamics was significant, but was only seen using GGFG peptide and not with the GGLFG peptide polymer. It can be speculated why there was an observed difference in effects between the two peptides. One possibility is that the GGFG moieties were able to weakly bind to FG-domain cross-links in a way that altered the dynamics of a putative Nup hydrogel structure, whereas GGLFG peptides would be expected to bind more strongly and not allow a rapid transfer of cross-links. These issues would be best resolved in future studies using copolymers created with more carefully controlled copolymer substitutions. For example, uniform low molecular weight polymers with exactly one, two, or more peptide groups would be useful to determine if the effects observed here were influenced by single vs multimer binding to Nups. An essential preliminary to further this work would be to characterize the exact binding properties of a test polymer with Nup proteins in vitro before evaluating their effects in living cells.

Conclusions

HPMA copolymers possessing a very wide range of chemical characteristics proved to have very little interaction with any macromolecular component in the cell and were specifically excluded from all membrane-limited subcellular compartments, with exception of the nucleus. All copolymers rapidly and evenly diffused throughout the cytoplasmic compartment following microinjection, and the smallest copolymer fractions also rapidly diffused into the nucleus. The exception to passive intracellular diffusion was the strongly cationic copolymer containing 20% MATC, a quaternary amine. This copolymer was found to localize specifically to microtubules from the cytoplasm over a period of 2–12 h.

Nuclear entry from the cytoplasm was dictated by size-limited passive diffusion through the NPC, however, small but significant differences in rates of nuclear import were observed for polymers with sizes near the molecular weight exclusion limit as a function of the charge and hydrophobicity of the copolymers. HPMA copolymers containing peptides with Nup cross-linking sequences were found to exert a significant and specific, though modest, effect on the kinetics of NPC transport. It was found that low molecular copolymers possessing GGFG pendant groups (but not GGLFG peptides) increased the molecular weight threshold for passive uptake through the NPC channel. This was observed for the 5% GGFG copolymer itself and with coinjected polymer acting as a nuclear exclusion marker. It was hypothesized that interactions with the GGFG copolymer may have altered the dynamics of

Nup cross-linking in the NPC channel rather than affecting any general conformational transition in the proteins' structure.

Supplementary Material

Refer to Web version on PubMed Central for supplementary material.

Acknowledgments

We thank Dr. C. Rodesch and K. Carney of the University of Utah Core Cell Imaging Facility for their assistance with cell microinjection, imaging, and image processing and Dr. K. Ullman for valuable discussions. The research was supported in part by NIH Grant CA51578 from NCI and the DoD Grant W81XWH-04-1-0900.

References and Notes

1. Kopeček J. Polim Med. 1977; 7:191–221. [PubMed: 593972]
2. Říhová B, Bilej M, Větvička V, Ulbrich K, Strohalm J, Kopeček J, Duncan R. Biomaterials. 1989; 10:335–342. [PubMed: 2765631]
3. Seymour LW, Duncan R, Strohalm J, Kopeček J. J Biomed Mater Res. 1987; 21:1341–1358. [PubMed: 3680316]
4. Harris JM, Martin NE, Modi M. Clin Pharmacokinet. 2001; 40:539–551. [PubMed: 11510630]
5. Říhová B, Ulbrich K, Kopeček J, Mančal P. Folia Microbiol. 1983; 28:217–227. [PubMed: 6873772]
6. Kopeček J. Ann NY Acad Sci. 1991; 618:335–344. [PubMed: 2006794]
7. Forrest ML, Gabrielson N, Pack DW. Biotechnol Bioeng. 2005; 89:416–423. [PubMed: 15627256]
8. Nan A, Croft SL, Yardley V, Ghandehari H. J Controlled Release. 2004; 94:115–127.
9. Cavallaro G, Mariano L, Salmaso S, Caliceti P, Gaetano G. Int J Pharm. 2006; 307:258–269. [PubMed: 16298091]
10. Satchi-Fainaro R, Duncan R, Barnes CM. Adv Polym Sci. 2006; 193:1–65.
11. Boussif O, Lezoualc'h F, Zanta MA, Mergny MG, Scherman D, Demeneix B, Behr JP. Proc Natl Acad Sci USA. 1995; 92:7297–7301. [PubMed: 7638184]
12. Aronov O, Horowitz AT, Gabizon A, Fuertes MA, Pérez JM, Gibson D. Bioconjugate Chem. 2004; 15:814–823.
13. Frederickson R. Nat Biotechnol. 1999; 17:739.
14. Chinnery PF, Taylor RW, Diekert K, Lill R, Turnbull DM, Lightowlers RN. Gene Ther. 2000; 7:813. [PubMed: 10822309]
15. D'Souza GG, Boddapati SV, Weissig V. Mitochondrion. 2005; 5:352–358. [PubMed: 16154389]
16. Filipovska A, Eccles MR, Smith RA, Murphy MP. FEBS Lett. 2004; 556:180–186. [PubMed: 14706847]
17. Muratovska A, Lightowlers RN, Taylor RW, Turnbull DM, Smith RAJ, Wilce JA, Martin SW, Murphy MP. Nucleic Acids Res. 2001; 29:1852–1863. [PubMed: 11328868]
18. Cuchelkar V, Kopečková P, Kopeček J. Mol Pharm. 2008; 5:776–786. [PubMed: 18767867]
19. Pante N, Kann M. Mol Biol Cell. 2002; 13:425–434. [PubMed: 11854401]
20. Paine PL, Moore LC, Horowitz SB. Nature. 1975; 254:109–114. [PubMed: 1117994]
21. Feldherr CM, Akin D. J Cell Sci. 1997; 110:3065–3070. [PubMed: 9365276]
22. Chen AA, Derfus AM, Khetani SR, Bhatia SN. Nucleic Acids Res. 2005; 33:e190. [PubMed: 16352864]
23. Krishnan VV, Lau EY, Yamada J, Denning DP, Patel SS, Colvin ME, Rexach MF. PLoS Comput Biol. 2008; 4:e1000145. [PubMed: 18688269]
24. Ribbeck K, Görlich D. EMBO J. 2001; 20:1320–1330. [PubMed: 11250898]
25. Ribbeck K, Görlich D. EMBO J. 2002; 21:2664–2671. [PubMed: 12032079]
26. Frey S, Richter RP, Görlich D. Science. 2006; 314:815–817. [PubMed: 17082456]

27. Frey S, Görlich D. Cell. 2007; 130:512–523. [PubMed: 17693259]
28. Bickel T, Bruinsma R. Biophys J. 2002; 83:3079–3087. [PubMed: 12496079]
29. Melčák I, Hoelz A, Blobel G. Science. 2007; 315:1729–1732. [PubMed: 17379812]
30. Kopeček J, Bažilová H. Eur Polym J. 1973; 9:7–14.
31. Minko T, Kopečková P, Kopeček J. Int J Cancer. 2000; 86:108–117. [PubMed: 10728603]
32. Koňák Č, Mrkvičková L, Nazarova O, Ulbrich K. Supramol Sci. 1998; 5:67–74.
33. Ulbrich K, Šubr V, Strohalm J, Plocová D, Jelínková M, Říhová B. J Controlled Release. 2000; 64:63–79.
34. Minko T, Kopečková P, Kopeček J. Pharm Res. 1999; 16:986–996. [PubMed: 10450921]
35. Luby-Phelps K, Mujumdar S, Mujumdar RB, Ernst LA, Gailbraith W, Wagoner AS. Biophys J. 1993; 65:236–242. [PubMed: 8369435]
36. Gribbon P, Hardingham TE. Biophys J. 1998; 75:1032–1039. [PubMed: 9675204]
37. Seksek O, Biwersi J, Verkman AS. J Cell Biol. 1997; 138:131–142. [PubMed: 9214387]
38. Pollack, GH. Cells, Gels, and the Engines of Life. Ebner; Seattle, WA: 2001.
39. Alber F, Dokudovskaya S, Veenhoff LM, Zhang W, Kipper J, Devos D, Suprapto A, Karni-Schmidt O, Williams R, Chait BT, Sali A, Rout MP. Nature. 2007; 450:695–701. [PubMed: 18046406]
40. Patel SS, Belmont BJ, Sante JM, Rexach MF. Cell. 2007; 129:83–96. [PubMed: 17418788]
41. Bhattacharyya B, Wolff J. Biochemistry. 1974; 13:2364–2369. [PubMed: 4831636]
42. Erickson HP, Voter WA. Proc Natl Acad Sci USA. 1976; 73:2813–2817. [PubMed: 1066692]
43. Koňák Č, Rathi RC, Kopečková P, Kopeček J. Macromolecules. 1994; 27:1992–1996.
44. Ben-Efraim I, Gerace L. J Cell Biol. 2001; 152:411–417. [PubMed: 11266456]
45. Pyhtila B, Rexach M. J Biol Chem. 2003; 278:42699–42709. [PubMed: 12917401]
46. Lim RY, Huang NP, Köser J, Deng J, Lau KH, Schwarz-Herion K, Fahrenkrog B, Aebi U. Proc Natl Acad Sci USA. 2006; 103:9512–9517. [PubMed: 16769882]
47. Rout MP, Aitchison JD, Magnasco MO, Chait BT. Trends Cell Biol. 2003; 13:622–628. [PubMed: 14624840]
48. Macara IG. Microbiol Mol Biol Rev. 2001; 65:570–594. [PubMed: 11729264]
49. Beck M, Medalia O. Histol Histopathol. 2008; 23:1025–1033. [PubMed: 18498078]
50. Yang W, Musser SM. J Cell Biol. 2006; 174:951–961. [PubMed: 16982803]
51. Dange T, Grünwald D, Grünwald A, Peters R, Kubitscheck U. J Cell Biol. 2008; 183:77–86. [PubMed: 18824568]

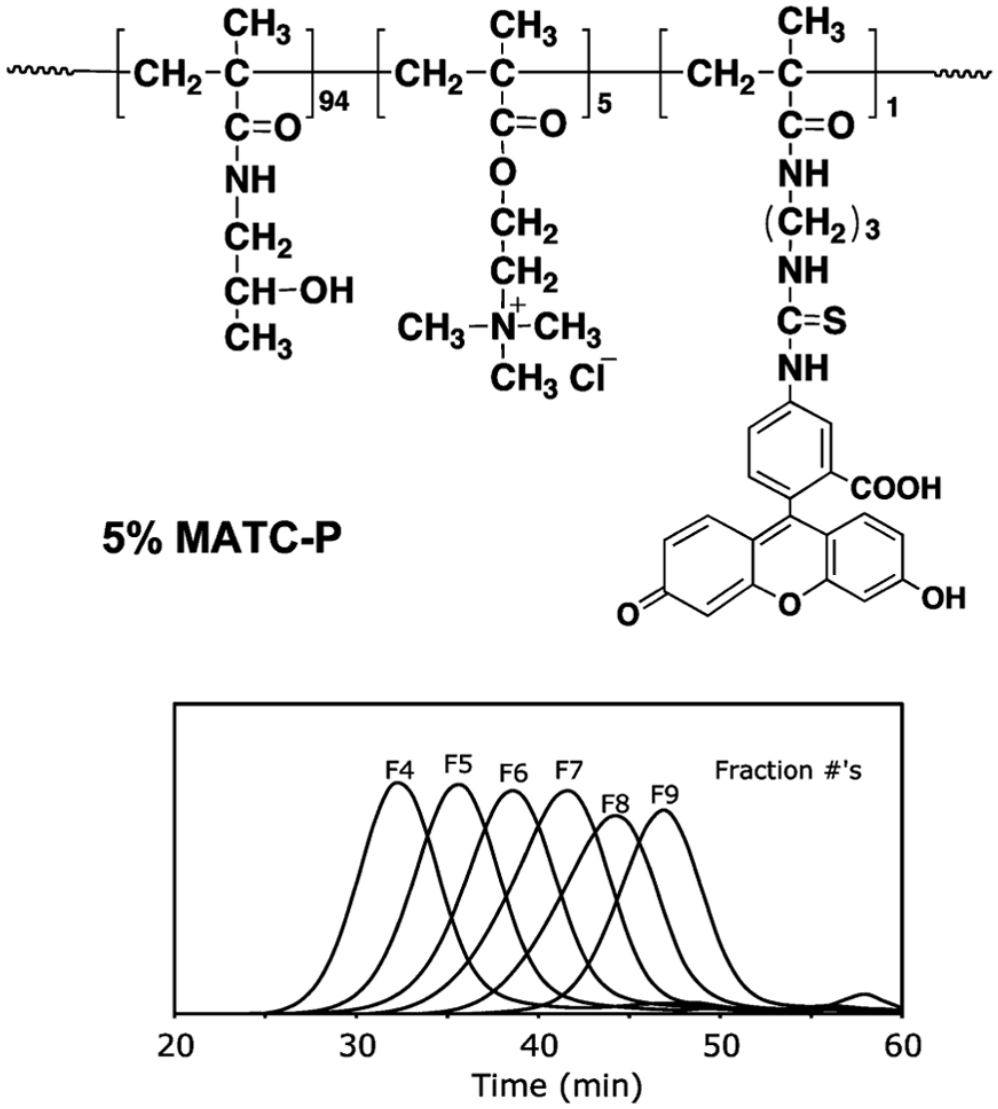

Figure 1.
Structure of 5% MATC-P and molecular weight profiles of copolymer fractions obtained by SEC.

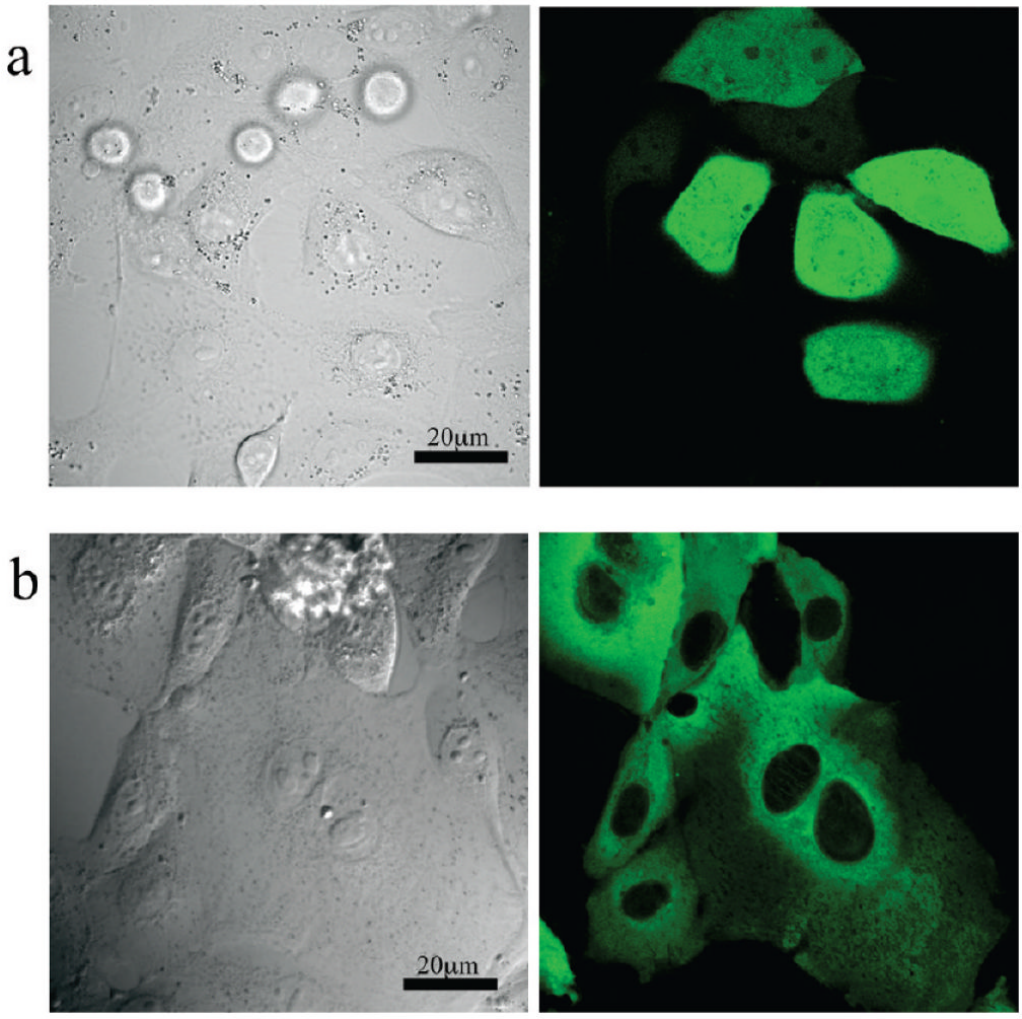

Figure 2.

Typical images from confocal laser scanning fluorescent microscopy (40× mag.) of live MDAH2774 ovarian carcinoma cells after microinjection with FITC-labeled polymers. The transmitted images are on the left. On the right, images represent fluorescent FITC-labeled copolymer. (a) 20% MATC-P-F8 (M_w = 23 kDa) 15 min after microinjection. Polymers under 25 kDa immediately dispersed in cytoplasm and nucleoplasm, but were excluded from other membrane-limited organelles. (b) 5% SEMA-P-F4 (M_w = 125 kDa) 24 h after microinjection. Polymers over 75 kDa remain excluded from the nuclei and all membrane-limited organelles. All polymers except for 20% MATC-P remained evenly dispersed throughout the cytoplasm and excluded from subcellular structures, as demonstrated in this example.

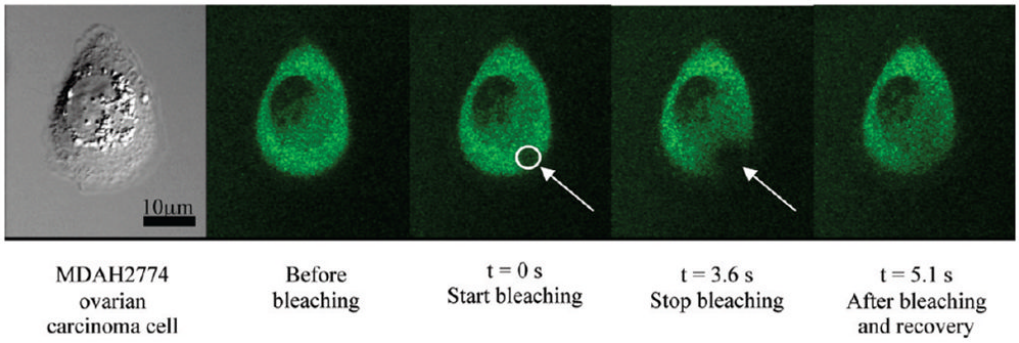

Figure 3.

Example of time-lapse imaging from FRAP. Here, MDAH2774 cells were microinjected with copolymer 5% MAA-P-F4 (M_w = 96 kDa) 2 h before the experiment. Area was bleached as indicated and cytosolic copolymer rediffused and restored equilibrium concentration within 3 s. The free diffusion in the cytoplasm of relatively high molecular weight copolymers was demonstrated.

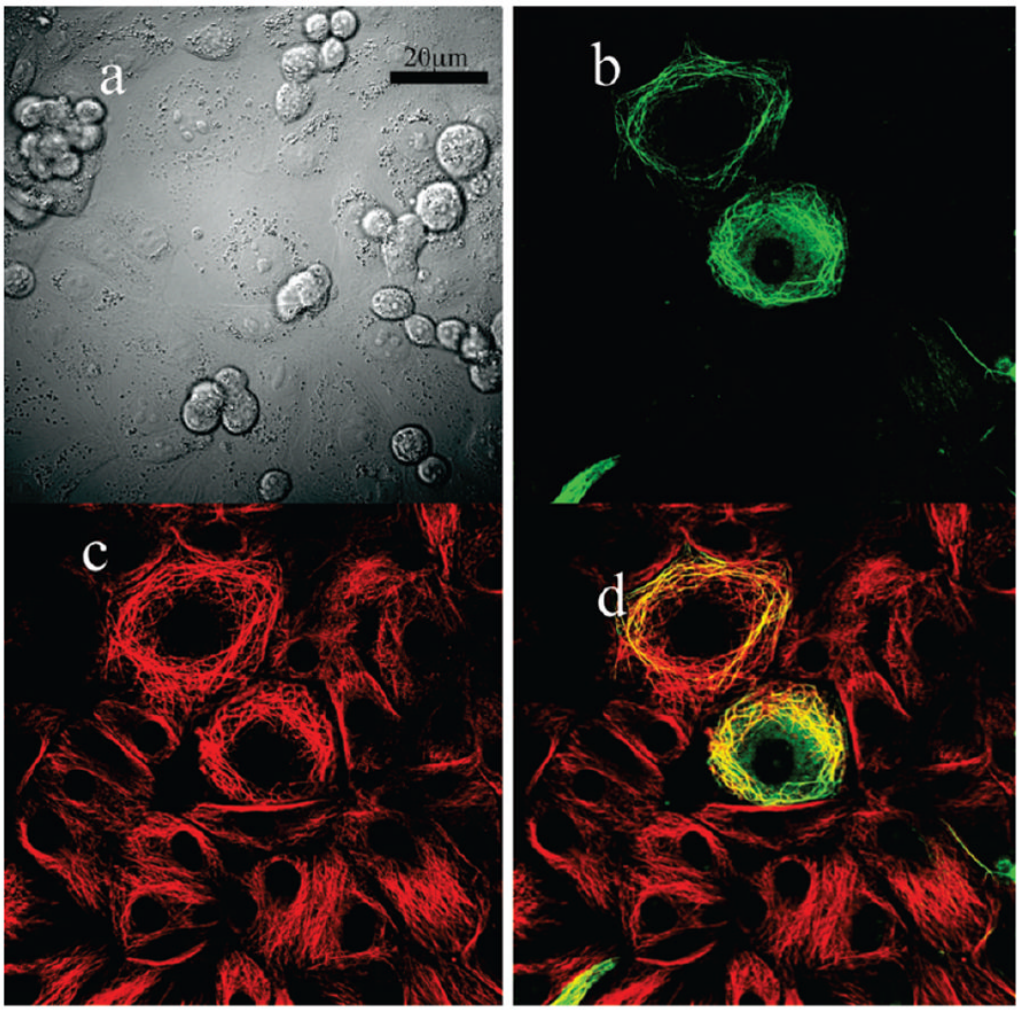

Figure 4.

Typical images of fixed MDAH2774 cells after microinjection with strongly cationic copolymer 20% MATC-P-F4 (M_w = 103 kDa), thereby demonstrating its localization on microtubules. Cells were microinjected with copolymer 24 h before fixation with 3% paraform-aldehyde. Microtubules were labeled using E7 antitubulin primary antibody, which was visualized using a goat antimouse 555-Alexafluor secondary antibody. The transmitted image is shown in (a). The green channel (b) is from the FITC-labeled copolymer and the red channel (c) shows microtubule staining. Overlay fluorescent image (d) demonstrated microtubule colocalization with the copolymer although some inhibition of the antitubulin antibody was evident when injected cell were compared with noninjected cells. Note: For these experiments large cells were selected to provide better images of subcellular structures.

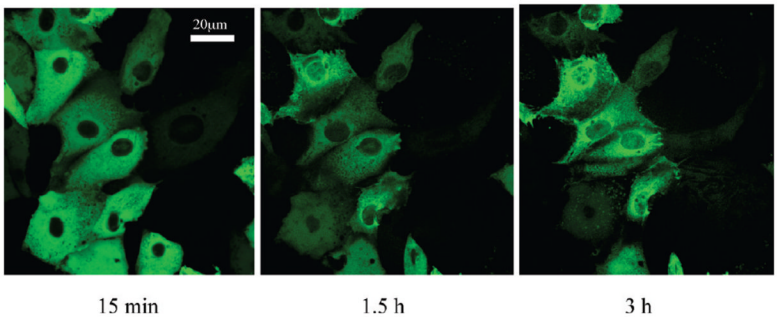

Figure 5.

Time series of a single z-slice of MDAH2774 ovarian carcinoma cells microinjected with 5% GFLG-P-F7 (M_w = 34 kDa; hydrophobic peptide) as a 1 mg/mL polymer solution in PBS. Green indicates microinjected polymer and entry into the nuclei is shown over time.

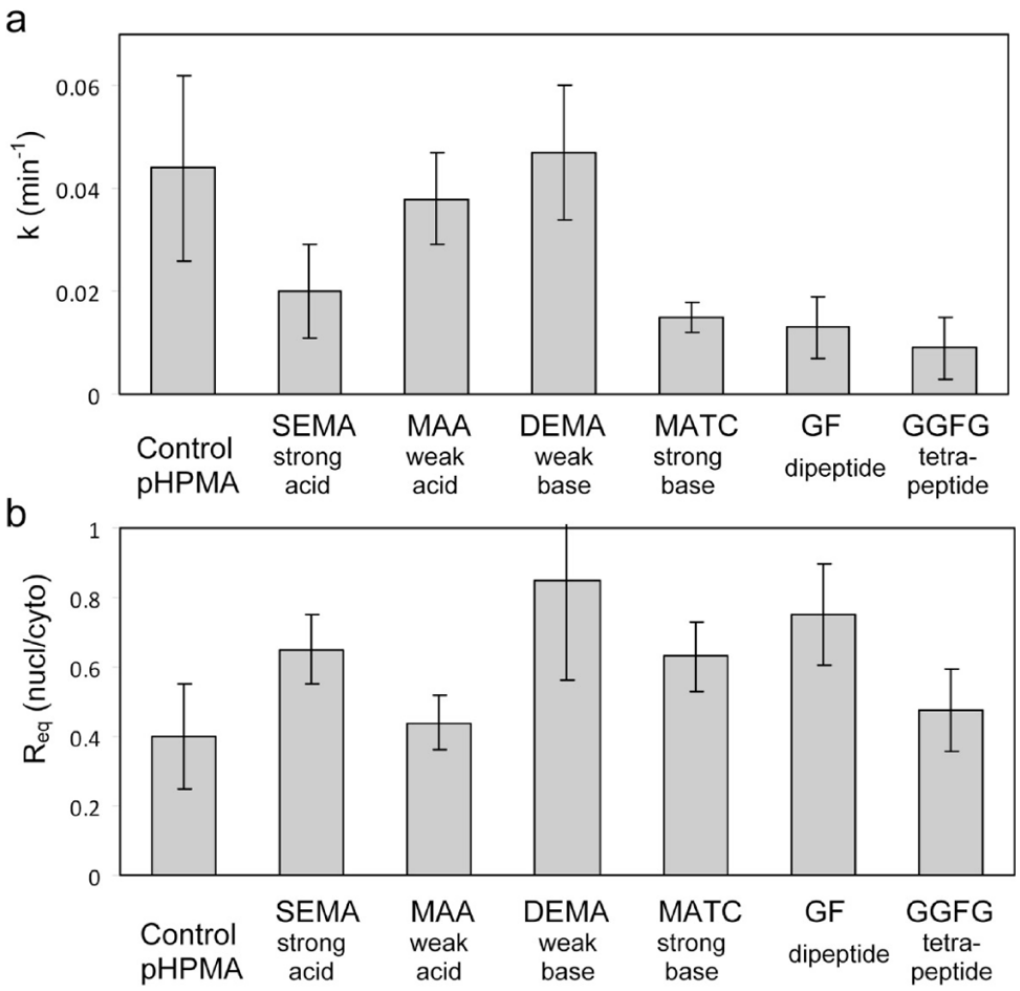

Figure 6.

(a) Nuclear uptake rate constants k (min^{-1}) for 5% copolymers. (b) Equilibrium nuclear/cytosol polymer concentrations (R_{eq}) for each copolymer type. (N = 5–9 cells). Error bars are standard errors (SE) for each calculated curve-fit.

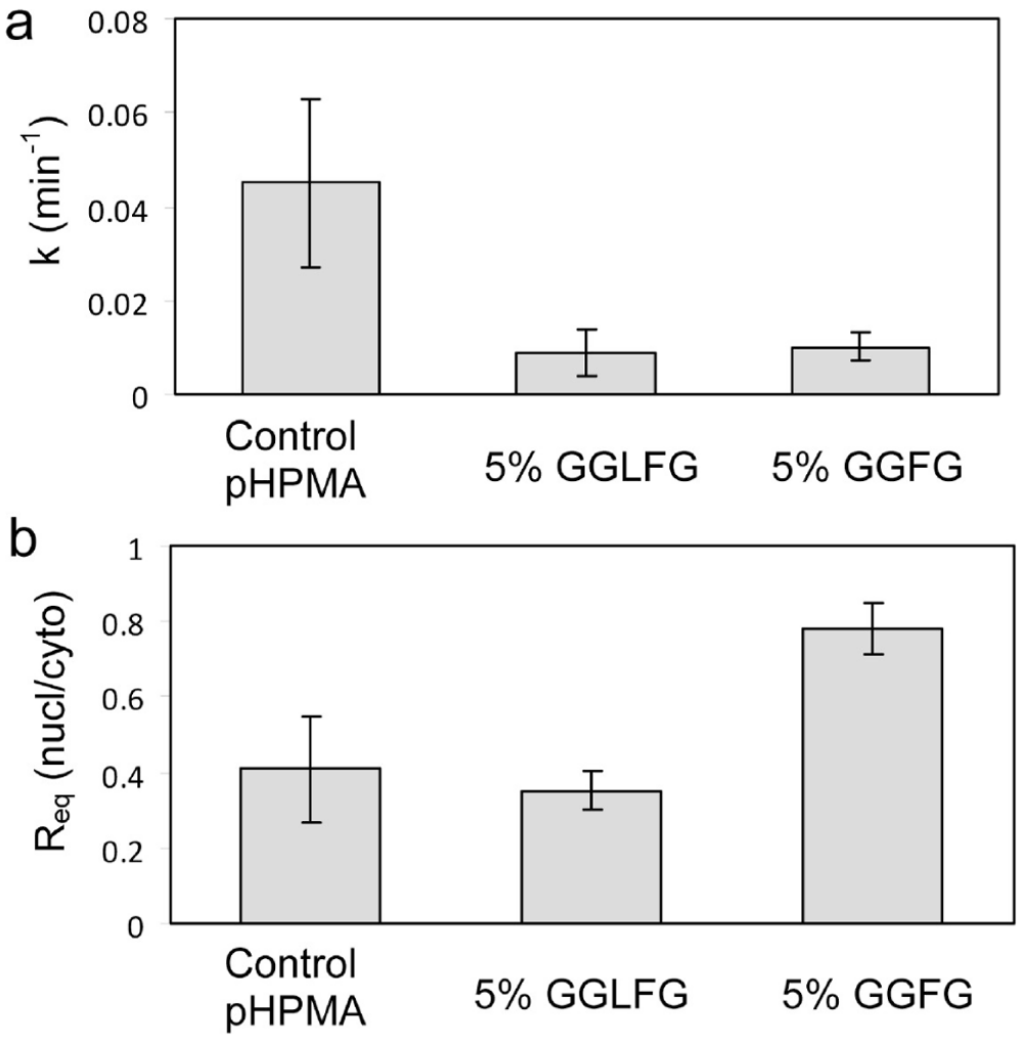

Figure 7.

(a) Nuclear uptake rate constants k (min^{-1}) for FG motif containing copolymers. (b) Equilibrium nuclear/cytosol polymer concentrations (R_{eq}) for FG copolymers. (N = 5–9 cells). Error bars are SE from each derivation.

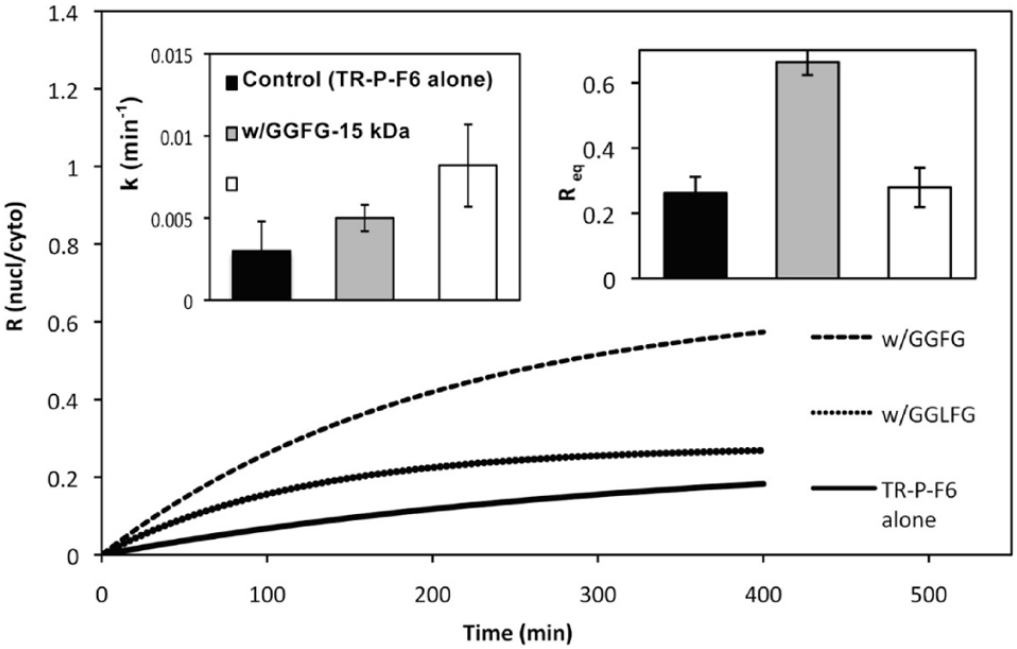

Figure 8.

Summary of the nuclear uptake kinetics of microinjected TR-P-F6. Inset graph on the left shows the nuclear uptake rate constants k (min^{-1}) and inset graph on the right shows the equilibrium nuclear/cytosol polymer concentrations (R_{eq}) for each copolymer type. Error bars in the inset are SE for each derivation.

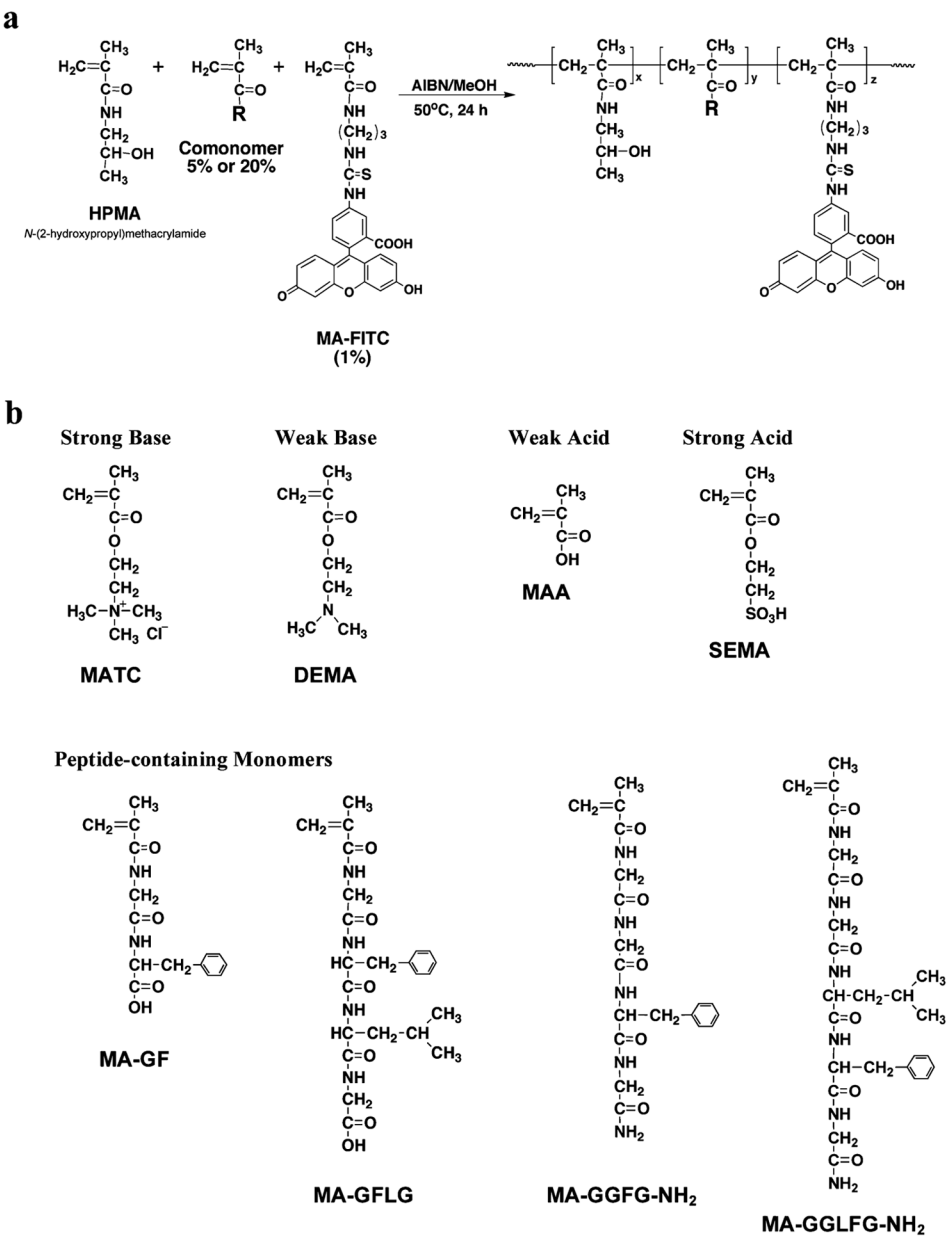

Scheme 1.

(a) General Synthetic Scheme for HPMA Copolymers; (b) Structure of Comonomers Used

Table 1

Characterization of HPMA Copolymers

		mole % in copolymer		M_w[c] (kDa)			fractionation								
							fraction 4			fraction 7			fraction 9		
polymer ID[a]	category	Mi	FITC[b]	M_w	M_n	M_w/M_n	M_w	M_n	M_w/M_n	M_w	M_n	M_w/M_n	M_w	M_n	M_w/M_n
5% SEMA-P	strong acid	3.9	0.78	41	27	1.5	125	106	1.2	30	27	1.1	14	13	1.1
20% SEMA-P		18.0	0.74	62	36	1.7	121	101	1.2	35	34	1.1	14	13	1.1
5% MAA-P	weak acid	4.8	0.67	53	31	1.7	96	87	1.1	46	42	1.1	15	14	1.1
20% MAA-P		18.2	0.65	68	40	1.7	100	89	1.1	37	31	1.2	17	15	1.1
5% GFLG-P	peptide	4.0	0.52	38	26	1.5	80	74	1.1	33	30	1.1	15	13	1.2
5% GF-P		4.6	0.59	41	26	1.6	111	95	1.2	43	38	1.1	15	13	1.2
5% DEMA-P	weak base	4.7	0.59	44	32	1.4	81	77	1.1	29	26	1.1	16	15	1.1
20% DEMA-P		19.1	0.58	49	31	1.6	99	93	1.1	30	30	1.0	12	11	1.1
5% MATC-P	strong base	4.4	0.55	53	31	1.7	105	96	1.1	37	30	1.2	15	14	1.1
20% MATC-P		16.5	0.58	50	30	1.7	103	93	1.1	40	34	1.2	16	13	1.2

[a] "P" denotes the HPMA copolymer backbone; the % refers to the concentration of the monomer Mi in feed; e.g., 5% SEMA-P refers to the copolymer prepared by copolymerization of 5 mol % of SEMA, 94 mol % HPMA, and 1 mol % of MA-FITC.

[b] Content of MA-FITC in the copolymer.

[c] Determined by size exclusion chromatography (SEC).

Table 2

Characterization of FG-Containing HPMA Copolymers

		mole % in copolymer		M_w[c] (kDa)			fractionation								
							fraction 6			fraction 7			fraction 9		
polymer ID	**Mi**	**Mi**	**FITC[b]**	M_w	M_n	M_w/M_n	M_w	M_n	M_w/M_n	M_w	M_n	M_w/M_n	M_w	M_n	M_w/M_n
5% GGLFG-P[a]	MA-GGLFG-NH_2	2.8	0.66	40	26	1.5				30	27	1.1	14	13	1.1
5% GGFG-P	MA-GGFG-NH_2	1.9	0.73	38	26	1.5				26	24	1.1	15	14	1.1
TR-P (exclusion marker; Texas Red labeled HPMA copolymer)							45	39	1.2	35	31	1.1			

[a] "P" denotes the HPMA copolymer backbone; the % refers to the concentration of the monomer Mi in feed; e.g., 5% GGLFG-P refers to the copolymer prepared by copolymerization of 5 mol % of MA-GGLFG-NH_2, 94 mol % HPMA, and 1 mol % of MA-FITC.

[b] Content of MA-FITC in the copolymer.

[c] Determined by size exclusion chromatography (SEC).